

# Impact of non-equilibrium chemical kinetics on communication blackout characterization for a hypersonic entry vehicle

By S. M. Jo<sup>†</sup> AND C. T. Williams

The present study provides detailed computational analysis of the impact of non-equilibrium chemical-kinetic models on the characterization of radio communication blackout around a hypersonic atmospheric entry vehicle to Mars. Species electronic master equations are coupled to the reactive Navier-Stokes equations to yield a high-fidelity representation of electronic energy transfer, which is critical to the free-electron productions and, thus, prediction of blackout in high-Mach flows. Comparisons with a conventional two-temperature model reveal that the state-resolved approach predicts significantly higher free-electron production, resulting in disparate trends in the expected signal attenuation. Motivated by these discrepancies, we propose improvements to the nominal two-temperature approach, informed by detailed master-equation analyses. Introducing physical source terms to the energy conservation equations, the proposed two-temperature modifications significantly improve the prediction of electron number densities in non-equilibrium conditions, without any significant increase in computational cost.

---

## 1. Motivation and objectives

In hypersonic flight, the high-temperature shock layers enveloping aerospace vehicles are subject to several finite-rate thermochemical processes, such as internal-energy excitation, chemical dissociation and ionization. Progression of the various thermochemical processes in the shock-heated, calorically non-perfect gas ultimately affects not only the aerothermal heating at the vehicle surface, but also the attenuation of communication signals by shock-layer free electrons (Park (1989)). This radio communication blackout hinders the exchange of information between ground control, satellites, and hypersonic vehicles, introducing significant uncertainty in space exploration mission design. For these atmospheric entry flows, thermochemical states remain strongly out of equilibrium, with the characteristic relaxation timescales comparable to that of convective transport. As such, accurate numerical predictions of communication blackout for hypersonic flight vehicles in these conditions rely sensitively on the fidelity of the chemical-kinetic modeling.

Existing studies on rovibrational energy transfer in hypersonic flows (Jo *et al.* (2022); Torres & Schwartzenruber (2024)), as well as dissociation (Venturi *et al.* (2020)) and ionization (Jo *et al.* (2019); Brandis *et al.* (2020)), have demonstrated strong coupling among the thermal and chemical non-equilibrium processes. However, existing studies on the numerical characterization of radio communication blackout phenomena have largely focused instead on the development of ray-tracing-based numerical frameworks (Giangaspero *et al.* (2023)), or the sensitivity to chemical reactions under a nominal two-temperature (2T) approach (Papajak *et al.* (2024)). Given the inherent equilibrium

<sup>†</sup> Department of Aerospace Engineering, Korea Advanced Institute of Science and Technology, Republic of Korea

assumption invoked in 2T modeling paradigms, their validity in accurately representing free-electron production remains unproven.

To characterize the sensitivity of computational blackout predictions, the present study details direct simulations of Martian atmospheric entry utilizing a fully coupled computational framework, comprising electronic master equations together with the reactive Navier-Stokes equations. Refining possible reaction pathways for high-lying energy levels near the ionization limit, the master-equation approach provides a higher-fidelity prediction of free-electron production relative than conventional 2T approximations. To assess the impact of this free-electron production on characterizations of radio communication blackout, the present study considers the entry flow around the Mars2020 capsule geometry, for which a severe blackout period has been identified (Morabito *et al.* (2021)). The fidelity of legacy 2T models in representing ionization processes is then evaluated via comparison with the state-resolved numerical simulations, in terms of both predicted electron number densities and signal attenuation. To rectify the identified deficiencies in the baseline 2T approach, a model improvement is then proposed by deriving self-consistent physical source terms, informed by state-resolved calculations.

The remainder of this report is organized as follows: Section 2 describes modeling details of the non-equilibrium processes, including the governing equations and the chemical-kinetic database. Section 3 summarizes key findings, highlighting the impact of the physical models in characterizations of radio communication blackout. Section 4 proposes an improved physical-modeling strategy informed by the master-equation approach, and finally, Section 5 provides concluding remarks.

## 2. Modeling of non-equilibrium chemical-kinetic processes

### 2.1. Conservation equations

A continuum description of thermochemical non-equilibrium is utilized in the present study, consisting of species electronic master equations coupled with the Navier-Stokes equations to enable a direct description of species non-Boltzmann electronic population distributions. For each bulk species (*e.g.* CO<sub>2</sub>) and selected species electronic states (*e.g.* N<sub>2</sub> (X<sup>1</sup>Σ<sub>g</sub><sup>+</sup>), N<sub>2</sub> (A<sup>3</sup>Σ<sub>u</sub><sup>+</sup>), etc.), the conservation of mass for component *i* reads

$$\frac{\partial \rho_i}{\partial t} + \nabla \cdot (\rho_i \mathbf{u}) = -\nabla \cdot (\rho_i \mathbf{U}_i) + \dot{w}_i, \quad (2.1)$$

where  $\rho_i$ ,  $\mathbf{U}_i$  and  $\mathbf{u}$  correspond to the component partial density, component diffusion velocity and bulk velocity vector, respectively. Formulated in terms of the number density,  $n_i$ , the chemical production rates,  $\dot{w}_i$ , are given by

$$\begin{aligned} \dot{w}_i|_{n_i} = & - \sum_j (k_{ij}^e n_i - k_{ji}^e n_j) n_e - \sum_j (k_{ij}^M n_i - k_{ji}^M n_j) n_M - (k_i^{I,e} n_i - k_i^{IR,e} n_+ n_e) n_e \\ & - (k_i^{D,e} n_i - k_i^{DR,e} n_A n_B) n_e - (k_i^{D,M} n_i - k_i^{DR,M} n_A n_B) n_M = \left( \frac{\partial n_i}{\partial t} \right)_{col}, \quad (2.2) \end{aligned}$$

where  $k$  denotes a reaction rate coefficient for a particular fundamental process. In this formulation, electronic-state-resolved excitation ( $k_{ij}^I$ ), de-excitation ( $k_{ji}^I$ ), ionization ( $k_i^I$ ), dissociation ( $k_i^D$ ) and recombination ( $k_i^{IR}$  and  $k_i^{DR}$ ) processes through electron (*e*) and heavy-particle (*M*) impacts are directly represented. As such, non-Boltzmann electronic-state distributions can be directly obtained by integrating Eq. (2.1). Together with the pseudo- and macroscopic species continuity equations, the numerical solutions likewise

entail integration of the momentum and energy conservation equations, under the approximation that rotational and vibrational energy modes remain in Boltzmann states characterized by the respective temperatures,  $T_{tr}$  and  $T_{eev}$ . In the case that the  $i$ -th component represents a bulk species,  $\dot{w}_i$  is directly evaluated with the baseline 2T model (Park (1989)).

The energy conservation equations are formulated in a manner closely resembling the nominal 2T approach, while excluding the species electronic energy modes from the electron-electronic-vibrational energy ( $E_{eev}$ ) pool, as the electronic energy is instead evolved according to the electronic master equations given by Eq. (2.2). The present formulation neglects the energy-exchange rates due to radiative transitions based on the findings of Brandis *et al.* (2020), resulting in only collisional contributions, as denoted by  $(\partial n_i / \partial t)_{col}$  in Eq. (2.2). In this formulation, thermodynamic properties are calculated directly from the partition function and its derivatives. Electronic contributions to the transport properties, such as viscosity and thermal conductivity, are first computed for the bulk species. Then, the species-specific properties are Boltzmann-distributed across the electronic states to estimate the state-specific components. Integration of the conservation equations is performed with the solver HEGEL (Munafò *et al.* (2024)), which is based on a multi-block structured finite-volume method.

## 2.2. Chemical-kinetic database

Two different chemical-kinetic databases for the Martian atmosphere have been constructed for the present study: the first for the baseline 2T model and the latter for the electronic-master-equation approach. Nineteen bulk species, N, O, C, CO, CO<sub>2</sub>, C<sub>2</sub>, CN, N<sub>2</sub>, NO, O<sub>2</sub>, NO<sup>+</sup>, CO<sup>+</sup>, CN<sup>+</sup>, C<sup>+</sup>, O<sub>2</sub><sup>+</sup>, O<sup>+</sup>, N<sup>+</sup>, N<sub>2</sub><sup>+</sup> and e<sup>-</sup>, are considered to describe the chemical-kinetic processes in the Martian atmosphere. The nominal 2T model largely consists of the reaction-rate coefficients from Johnston *et al.* (2012), but the previously missing charged-species interactions have now been included in the present work. In total, 49 chemical reactions among the bulk species, representing heavy-particle and electron-impact dissociation, neutral and charge exchange and associative or electron impact ionization, are considered in the baseline 2T model.

In the electronic-master-equation approach, the chemical-kinetic processes are extended to the pseudo-species (*i.e.* the electronic states) to describe electronic-energy transfer and ionization with improved physical self-consistency. The considered electronic energy states are presented in Table 1; the electronic-energy modes of the bulk species not included in Table 1 are assumed to be Boltzmann-distributed at the temperature  $T_{eev}$ . In total, 71 species continuity equations, including both pseudo- and macroscopic species, are considered in the master-equation model. The electronic levels of the atomic species, N, O and C, are grouped based on the multi-group maximum entropy principle (Liu *et al.* (2015)) to reduce the computational cost, decreasing the size of the mass matrix for the system. As such, 8 states are utilized to collectively represent 38, 32 and 22 electronic levels for atomic N, O and C, respectively.

The state-specific collisional transition rate coefficients in Eq. (2.2) are taken from several sources (Park (2008*a,b*); Johnston *et al.* (2012); Jo *et al.* (2019), *etc.*) and have been validated directly against non-equilibrium radiation measurements (Cruden *et al.* (2012)). In total, 1172 kinetic processes are modeled in the electronic-state-resolved approach.

---

|                             |   |
|-----------------------------|---|
| N                           | 1 – 38 grouped into 1 – 8   |
| O                           | 1 – 32 grouped into 1 – 8   |
| C                           | 1 – 22 grouped into 1 – 8   |
| CO                          | 1 – 6 ( $X^1\Sigma^+$ , $a^3\Pi$ , $a'^3\Sigma^+$ , $d^3\Delta$ , $e^3\Sigma^-$ , $A^1\Pi$ )                      |
| C <sub>2</sub>              | 1 – 7 ( $X^1\Sigma_g^+$ , $a^3\Pi_u$ , $b^3\Sigma_g^-$ , $A^1\Pi_u$ , $c^3\Sigma_u^+$ , $d^3\Pi_g$ , $C^1\Pi_g$ ) |
| CN                          | 1 – 5 ( $X^2\Sigma^+$ , $A^2\Pi$ , $B^2\Sigma^+$ , $a^4\Sigma^+$ , $D^2\Pi$ )                                     |
| N <sub>2</sub>              | 1 – 6 ( $X^1\Sigma_g^+$ , $A^3\Sigma_u^+$ , $B^3\Pi_g$ , $W^3\Delta_u$ , $B'^3\Sigma_u^-$ , $a'^1\Sigma_u^-$ )    |
| N <sub>2</sub> <sup>+</sup> | 1 – 5 ( $X^2\Sigma_g^+$ , $A^2\Pi_u$ , $B^2\Sigma_u^+$ , $D^2\Pi_g$ , $C^2\Sigma_u^+$ )                           |
| O <sub>2</sub>              | 1 – 4 ( $X^3\Sigma_g^-$ , $a^1\Delta_g$ , $b^1\Sigma_g^+$ , $c^1\Sigma_u^-$ )                                     |
| NO                          | 1 – 5 ( $X^2\Pi$ , $a^4\Pi$ , $A^2\Sigma^+$ , $B^2\Pi$ , $b^4\Sigma^-$ )  |

---

TABLE 1. Species electronic levels considered in the electronic master equation.

### 3. Influence of chemical-kinetic models

To assess the sensitivity of blackout predictions to non-Boltzmann chemical kinetics, the hypersonic flow around the Mars2020 capsule geometry is numerically simulated using the two different physical models described in Section 2. The physical models are integrated into the physico-chemical library PLATO (Munafò & Panesi (2023)) to describe the fundamental chemical-kinetic processes with flexibility. Apart from the chemical production source terms, as well as the transport of the additional pseudo-species, the discretization and numerical solution procedures of the conservation equations remain fully consistent for both physico-chemical models. Numerical integration of the conservations equations is performed with a fourth-order accurate explicit time integration scheme, inviscid fluxes are evaluated with a second-order accurate AUSM<sup>+</sup>-UP (Liou (2006)) scheme and diffusive fluxes are evaluated with second-order central differencing. Geometric representation of the entry vehicle is provided by a multi-block structured grid topology, which includes the forebody and the wake region around the capsule, resulting in the construction of five blocks. In total, 260,180 cells are included in the computational domain. The freestream conditions are taken from the Mars2020 mission scenario, in which severe communication blackout has been identified: The chemical composition is 96% CO<sub>2</sub> and 4% N<sub>2</sub> on a molar basis, while the flight speed and ambient static pressure are given by 5.3 km/s and 4.43 Pa, respectively. As the focus of the present study is the role of non-equilibrium ionization kinetics, transition to turbulence is precluded in the present calculations on the basis of the fully two-dimensional axisymmetric representation; analysis of the potential coupling between turbulent fluctuations and ionization processes is therefore deferred to future work.

Predicted free-electron number densities ( $n_{e-}$ ) are provided in Figure 1 for both the baseline 2T and state-resolved electronic-master-equation (StS) models, together with the definitions of the four lines-of-sight (LOS) relevant for radio communication. In particular, LOS-1 and LOS-2 correspond to the stagnation and shoulder lines, while LOS-3 and LOS-4 transect the wake region where the radio communication blackout is usually measured in flight experiments (Morabito *et al.* (2021)). Variation of the free-electron number densities along these LOS is presented in Figure 2 as a function of distance from the vehicle surface,  $s$ . At the selected conditions along the flight trajectory, the StS approach predicts a significantly larger degree of free-electron production, resulting in more severe attenuation of the communication signal. In the vicinity of the wake, the StS-predicted  $n_{e-}$  exceeds the critical value,  $n_{e-}^c = 2 \times 10^{15} \text{ m}^{-3}$ , estimated based on the local refractive index. On the basis of the StS results, then, a radio signal propagating

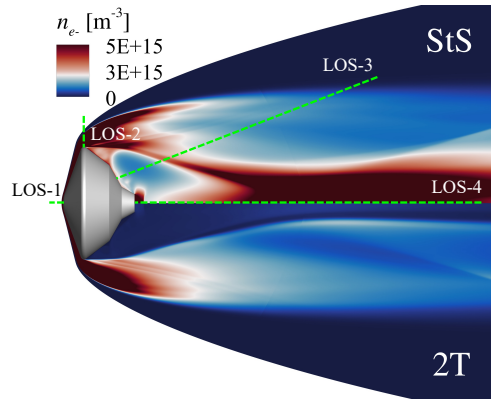


FIGURE 1. Comparison of free-electron number density distributions between the electronic-master equation (top) and nominal 2T (bottom) models. The various lines-of-sight (LOS) are represented as green dashed lines.

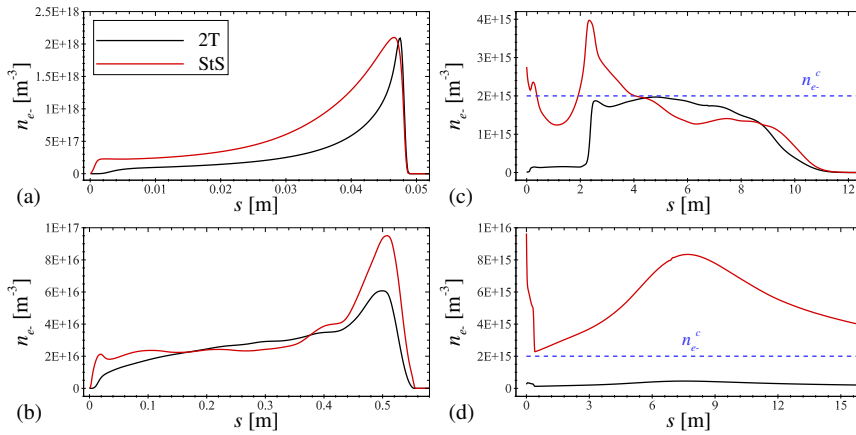


FIGURE 2. Comparisons of the free-electron profiles along with the lines-of-sight. (a) LOS-1, (b) LOS-2, (c) LOS-3 and (d) LOS-4. The critical electron number density is denoted by the blue dashed lines.

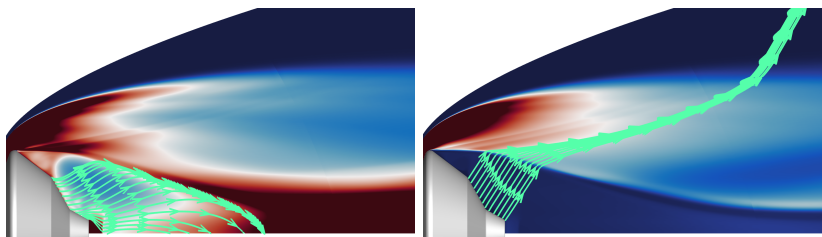


FIGURE 3. Signal propagation (green solid lines) overlaid on the free-electron number density contours, as predicted by the electronic-master-equation (left) and nominal 2T (right) approaches.

from the vehicle antenna is expected to be refracted, hindering any satellite communication through the wake. In contrast, the predicted peak electron number density from the 2T approach remains below its critical value in the vehicle wake, erroneously implying

that radio communication would remain relatively unimpeded by the ionization processes. This discrepancy of the reduced-fidelity 2T predictions with the corresponding StS results can in part be attributed to the inherent physical assumptions that the energy removal by dissociation/ionization processes is effectively nonpreferential and that the internal-energy modes, though characterized by separate temperatures, remain well-described by Boltzmann statistics. The StS does not rely on this equilibrium approximation for the electronic energy, and hence more accurately captures the preferential behavior of ionization, dissociation, and electronic-energy-transfer processes. At these atmospheric entry conditions, accurately representing this preferential behavior proves crucial, as will be shown in Section 4. Therefore, the legacy 2T approach introduces significant errors in its predictions of the free-electron number densities in the wake.

To directly assess the impact of predicted free-electron number densities on signal propagation from the vehicle's backshell antenna, numerical solution of the Eikonal equation is performed with a finite-volume approach utilizing an unstructured grid topology with the same geometry as the entry flow-field computations. In the present study, the radio frequency is taken to be a constant value, uniformly distributed along the vehicle's backshell for simplicity. Figure 3 presents the simulated radio-signal attenuation around the wake region given the predicted electron number densities from the 2T and StS approaches. In the case of the nominal 2T model, the emitted signal is able to cross the shock layer, owing to the relatively lower predicted electron number densities. For the StS approach, however, the signal is shown to experience significant attenuation instead, indicating that a high-fidelity description of non-equilibrium chemical kinetics proves crucial for accurate radio communication blackout characterization at these atmospheric entry conditions.

#### 4. Physics-informed modification to the 2T model

Based on the discrepancies identified in Section 3, we now turn to improving the self-consistency of the nominal 2T model. This is achieved by leveraging physical information from electronic-master-equation simulations to provide a modification to the 2T model. The model improvements are realized by parameterizing electronic non-Boltzmann behavior in such a way that it can be embedded within a standard 2T framework. The modified 2T source terms therefore take the form

$$\dot{w}_{eev}^* = \dot{w}_{eev} + \sum_i \frac{E_{el,i}(T_{tr}) - E_{el,i}(T_{eev})}{\tau_{el-t}} + \sum_r^{R_{EI}} \omega_r I_r N_a \epsilon_s^{I,e} + \sum_r^{R_{ED}} \omega_r D_r N_a \epsilon_s^{D,e}, \quad (4.1)$$

where  $\dot{w}_{eev}^*$  and  $\dot{w}_{eev}$  are the modified and the nominal production rates of the electron-electronic-vibrational energy pool,  $E_{eev}$ . The second right-hand-side term describes energy transfer between the species electronic ( $E_{el}$ ) and translational energy modes, approximated as a first-order rate formulation with relaxation time parameter  $\tau_{el-t}$ . The third and fourth terms model the preferential behavior of the electron impact ionization and dissociation by introducing the average electronic energy removal ratios,  $\epsilon_s^{I,e}$  and  $\epsilon_s^{D,e}$ , where  $\omega_r$  is the reactive source term for reaction  $r$ .  $R_{EI}$  and  $R_{ED}$  denote the reactions sets for electron-impact ionization and dissociation, respectively.  $I_r$ ,  $D_r$  and  $N_a$  are the species ionization and dissociation potentials for species  $r$ , and Avogadro's number, respectively.

An ensemble of zero-dimensional state-resolved simulations is performed to simulate the thermal relaxation of the electronic energy modes, from which the characteristic re-

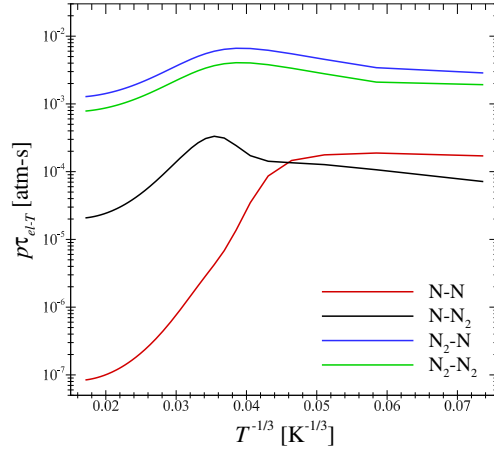


FIGURE 4. Characteristic electronic-translational energy transfer relaxation time  $p\tau_{el-t}$ .

relaxation times  $p\tau_{el-t}$  can be determined utilizing *e-folding*. These characteristic electronic relaxation times are provided in Figure 4 as a function of the translational temperature for the selected collision pairs in the Martian atmosphere. To represent the strongly non-monotonic behavior in  $p\tau_{el-t}$  with respect to translational temperature, a five-parameter curve-fitting approach, typically employed for describing equilibrium constants (Park (1989)), is utilized. The average electronic energy removal fractions for electron-impact ionization, as well as dissociation by the free-electron and heavy-particle impacts, are presented in Figure 5. These parameters represent the energy loss/gain, compared to the average energy potentials (*i.e.* ionization and dissociation potentials), during the particular chemical reactions.  $\epsilon_s^D$  is shown to approach a plateau in the high-temperature region, whereas  $\epsilon_s^I$  remains monotonically decreasing. Underlying the evaluation of these energy removal ratios is the assumption that the electronic-state populations are in a quasi-steady state (QSS) (Park (1989)), with Figure 6 comparing the electron-impact ionization rate coefficients with the literature data (Park (1989); Gokcen (2007)). The QSS rate coefficients  $k_{QSS}^{I,e}$  differ from factor 2 to two orders of magnitude compared with the reference data. By implementing the present QSS rate coefficients into the modified 2T model, then, one can replicate the corresponding chemical-reactive source terms of the StS approach.

Incorporating both the electronic relaxation and preferential energy release terms into Eq. (4.1) to construct the modified 2T model, preliminary verification is performed in a pure-nitrogen system, with both compressing (*i.e.* shock-heated) and expanding (*i.e.* recombining) scenarios. In the compression case, the spatial marching initial conditions are specified following the Rankine-Hugoniot relations for a 15 km/s normal shock in 5 Pa. Meanwhile, in the recombining case, a 0D isothermal chemical reactor at 4000 K is initialized with a non-equilibrium temperature of 20 000 K, replicating the thermodynamic states observed in the wake region. The computational results for both the shock-heated and recombining cases are presented in Figure 7, confirming that the additional physical source terms, informed by the StS approach, improve the predictive accuracy of the 2T model framework in describing the non-equilibrium behavior of the electronic energy transfers. The mole fractions of the free-electron  $X_e$  and the charged species are better reproduced by the modified 2T model, without incurring any significant increase

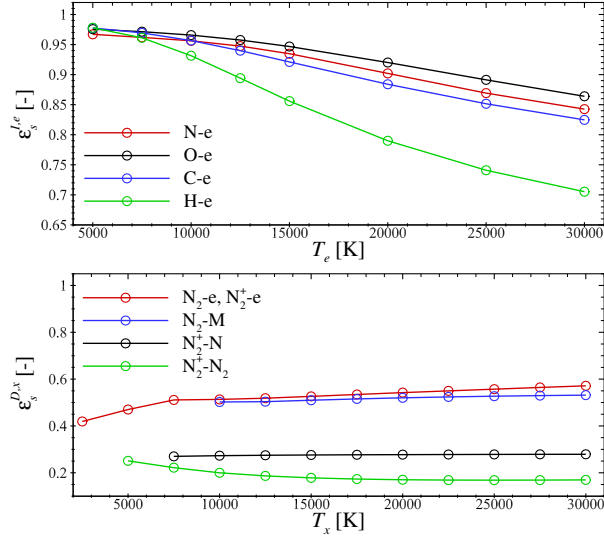


FIGURE 5. Expected electronic-energy removal ratios due to electron-impact ionization (top), as well as electron and heavy-particle impact dissociation (bottom).

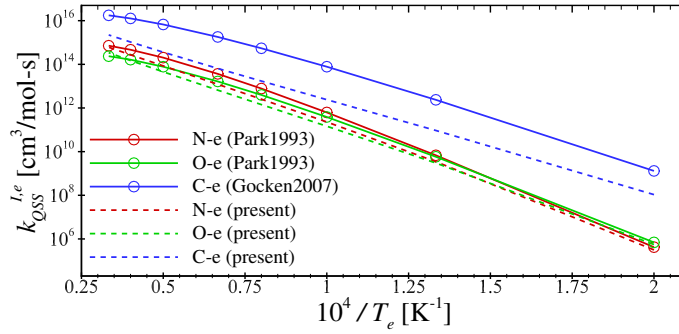


FIGURE 6. Comparison of the macroscopic electron-impact ionization rate coefficients.

in computational cost. Nevertheless, a certain level of discrepancy still persists (*e.g.*  $x$  near 0.0015 m in the top panels of Figure 7) that may arise from the inherent physical approximations of the 2T model, namely, assuming equilibrium between the species electronic and free-electron energy modes. Assessing the relative impact of intrinsically non-Boltzmann effects relative to electronic/electron non-equilibrium requires further investigation and will be the focus of future efforts.

## 5. Conclusions

This work presents an in-depth analysis of the influence of non-equilibrium chemical-kinetic models on the characterization of radio communication blackout around a hypersonic vehicle entering the Martian atmosphere. Detailed physico-chemical modeling of the highly ionized flow is realized by combining the compressible Navier-Stokes equations with state-resolved master-equations to describe ionization and species electronic energy transfer. In comparison with this state-resolved treatment of the electronic energy

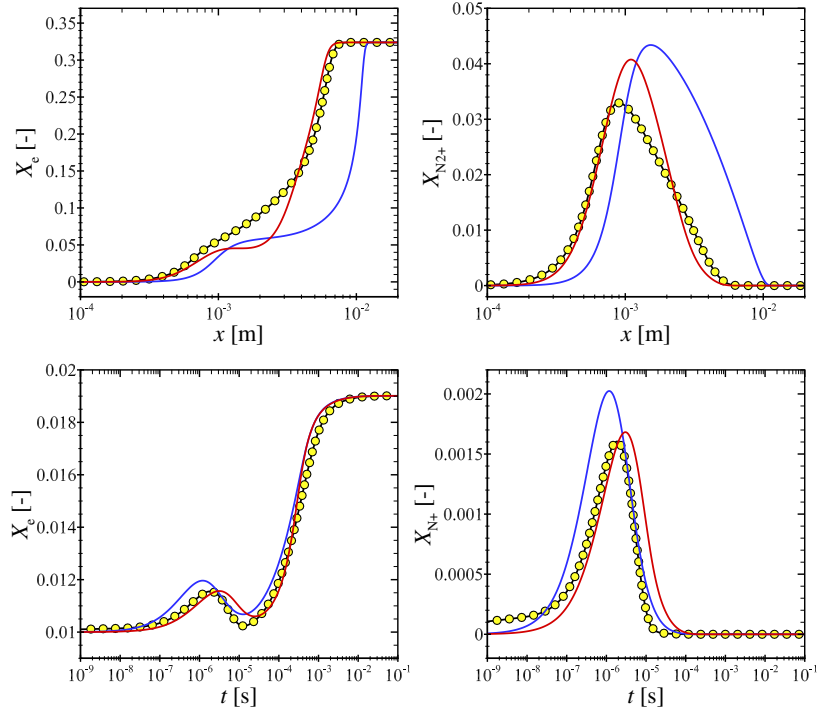


FIGURE 7. Verification of the modified 2T model for the compressing (top, post-normal shock) and expanding (bottom, 0D isothermal reactor) scenarios. The StS reference results are represented by black solid lines with yellow circles, while the modified and baseline 2T approaches are denoted by red and blue solid lines, respectively.

modes, the standard 2T approach is shown to significantly mispredict free-electron production and, as a result, communication blackout. To address this limitation, a series of physics-informed modifications are introduced to the source terms in the non-equilibrium energy conservation equation, informed by the state-resolved master equation analyses. Further numerical simulations ultimately demonstrate significant improvements in the predictive accuracy of the modified 2T model in terms of charged-species concentrations in hypersonic plasmas.

#### Acknowledgments

We are grateful for support from the Center for Turbulence Research through the Summer Program. S. M. J. acknowledges X. A. Vallespir, M. Panesi and A. Munafò for providing useful discussions and access to the solvers.

#### REFERENCES

- BRANDIS, A. M., SAUNDERS, D., JOHNSTON, C., CRUDEN, B. & WHITE, T. 2020 Radiative heating on the after-body of martian entry vehicles. *J. Thermophys. Heat Tr.* **34**, 66–77.
- CRUDEN, B. A., PRABHU, D. & MARTINEZ, R. 2012 Absolute radiation measurement in Venus and Mars entry conditions. *J. Spacecraft Rockets* **49**, 1069–1079.
- GIANGASPERO, V. F., SHARMA, V., LAUR, J., THOEMEL, J., MUNAFÒ, A., LANI, A.

- & POEDTS, S. 2023 3D ray tracing solver for communication blackout analysis in atmospheric entry missions. *Comp. Phys. Commun.* **286**, 108663.
- GOKCEN, T. 2007 N<sub>2</sub>-CH<sub>4</sub>-Ar chemical kinetic model for simulations of atmospheric entry to Titan. *J. Thermophys. Heat Tr.* **21**, 9–18.
- JO, S. M., KWON, O. J. & KIM, J. G. 2019 Electronic-state-resolved analysis of high-enthalpy air plasma flows. *Phys. Rev. E* **100**, 033203.
- JO, S. M., VENTURI, S., SHARMA, M. P., MUNAFÒ, A. & PANESI, M. 2022 Rovibrational-specific QCT and master equation study on N<sub>2</sub>(X<sup>1</sup>Σ<sub>g</sub><sup>+</sup>)+O(<sup>3</sup>P) and NO(X<sup>2</sup>Π) + N(<sup>4</sup>S) systems in high-energy collisions. *J. Phys. Chem. A* **126**, 3273–3290.
- JOHNSTON, C., BRANDIS, A. & SUTTON, K. 2012 Shock layer radiation modeling and uncertainty for Mars entry. *AIAA Paper* **2012-2866**.
- LIU, M.-S. 2006 A sequel to AUSM, Part II: AUSM<sup>+</sup>-up for all speeds. *J. Comput. Phys.* **214**, 137–170.
- LIU, Y., PANESI, M., SAHAI, A. & VINOKUR, M. 2015 General multi-group macroscopic modeling for thermo-chemical non-equilibrium gas mixtures. *J. Chem. Phys.* **142**.
- MORABITO, D. D., KOBAYASHI, M. M., KRASNER, S., BRUVOLD, K., OKINO, C., KAHAN, D., LEE, C., OUDRHIRI, K., LAY, N., SKLYANSKIY, E., LITTON, D. & JOHNSON, M. A. 2021 Insight communications degradation during peak heating phase of atmospheric entry. *J. Spacecraft Rockets* **58**, 856–864.
- MUNAFÒ, A., KUMAR, S., JO, S. M. & PANESI, M. 2024 Hegel: a high-fidelity flexible software for hypersonics and plasma simulations. In *AIAA Scitech 2024 Forum*, p. 0449.
- MUNAFÒ, A. & PANESI, M. 2023 Plato: a high-fidelity tool for multi-component plasmas. In *AIAA Aviation 2023 Forum*, p. 3490.
- PAPAJAK, E., HEDGES, T., NAUGHTON, C. & SAUNDERS, D. 2024 Improved chemistry and attenuation models for communication blackout simulation during Mars 2020 entry. In *AIAA Science and Technology Forum and Exposition (2024 AIAA SciTech Forum)*.
- PARK, C. 1989 *Nonequilibrium Hypersonic Aerothermodynamics*. New York: John Wiley and Sons.
- PARK, C. 2008a Rate parameters for electronic excitation of diatomic molecules I. Electron-impact processes. In *46th AIAA Aerospace Sciences Meeting and Exhibit*, p. 1206.
- PARK, C. 2008b Rate parameters for electronic excitation of diatomic molecules II. Heavy particle-impact processes. In *46th AIAA Aerospace Sciences Meeting and Exhibit*, p. 1446.
- TORRES, E. & SCHWARTZENTRUBER, T. E. 2024 Characteristic vibrational and rotational relaxation times for air species from first-principles calculations. *J. Thermophys. Heat Tr.* pp. 1–27.
- VENTURI, S., SHARMA, M. P., LOPEZ, B. & PANESI, M. 2020 Data-inspired and physics-driven model reduction for dissociation: Application to the O<sub>2</sub> + O system. *J. Phys. Chem. A* **124**, 8359–8372.